Available online at www.sciencedirect.com

ScienceDirect

Advances in Space Research 59 (2017) 2279–2294

ADVANCES IN SPACE RESEARCH (a COSPAR publication)

www.elsevier.com/locate/asr

Seasonal characteristics of COSMIC measurements over Indian sub-continent during different phases of solar activity

Malini Aggarwal [a,*], D.K. Sharma [b]

[a] Indian Institute of Geomagnetism, Mumbai 410218, India
[b] Department of Physics, Manav Rachna University, Faridabad, India

Received 10 October 2016; received in revised form 20 January 2017; accepted 8 February 2017
Available online 16 February 2017

Abstract

The seasonal characteristics of F2 region is investigated using peak electron density (NmF2) and corresponding altitude (hmF2) measurements obtained by COSMIC observations over Indian sub-continent (Geog. 5–40°N and 60–100°E) for the complete mission during the solar cycle 24 (Apr, 2006–Dec, 2013). A stronger EIA is observed in summer and winter during high solar activity whereas occurs in equinoxes during all levels of solar activity. The noontime winter anomaly in NmF2 is absent/weaker during low (2006–2009)/high (2010–2013) solar activity over equator whereas is stronger in low and moderate solar activity (2006–2007 and 2010–2011) but absent in minimum and maximum (2008–2009 and 2012–2013) solar activity over low-latitude respectively. The higher hmF2 is observed over the equator throughout the day (equator: 230–415 km and low-latitude: 220–340 km). The observed parameters, NmF2 and hmF2 are compared with the IRI-modeled values using CCIR and URSI options. The comparison exhibits a higher discrepancy in NmF2 in night-time and morning for equatorial and lower discrepancy for the whole day over the low-latitude whereas smaller (<20%) discrepancy exists in the hmF2 throughout the day using both IRI options. In conclusion, we found CCIR option in more agreement to the observed values for both equatorial and low-latitude regions respectively.

Keywords: NmF2; hmF2; COSMIC; Ionosphere; IRI-2012

1. Introduction

The earth's ionosphere is primarily formed by the photo-ionization of the upper atmosphere by the solar EUV and X-ray radiations. As a result, ionospheric parameters (e.g. electron density, electron and ion temperatures, peak electron density (NmF2), altitude corresponding to NmF2 (hmF2), ion composition and total electron content, (TEC)) also varies with the solar-cycle (e.g., Kawamura et al., 2002; Sharma et al., 2005, 2010; Aggarwal et al., 2007, 2009, etc.). The ionosphere undergoes complex seasonal variabilities which is not fully understood and various factors like solar zenith angle, thermospheric neutral composition, neutral winds, electric fields, etc., have been considered to explain them (e.g. Pavlov and Pavlova, 2005; Richards, 2001; Rishbeth et al., 2000; Kawamura et al., 2002; Rama Rao et al., 2006). The behavior of the ionospheric plasma density also deviates from the solar zenith angle dependence and generates anomalies in the F2 layer (>150 km altitude). The well known anomalies are: winter anomaly (also called the seasonal anomaly), semiannual anomaly and annual anomaly (also called the annual asymmetry (AI) or non-seasonal anomaly). The winter anomaly is a phenomenon during which the daytime electron density at F-peak altitude (NmF2) is higher in winter than summer. The semiannual anomaly is a phenomenon of higher NmF2 during equinoxes than solstices.

* Corresponding author.
E-mail address: asmalini@rediffmail.com (M. Aggarwal).

http://dx.doi.org/10.1016/j.asr.2017.02.018
0273-1177/

The annual anomaly is a phenomenon of higher NmF2 during the December solstice than June solstice when NmF2 is combined from both northern and southern hemispheres. The causes of these anomalies are still not known and are an ongoing research but changes in the chemical compositions have been found to be reasonable to explain these anomalies. The winter anomaly is due to the thermospheric composition differences between summer and winter which is caused by the prevailing upwelling of molecular rich air in the summer hemisphere and the downwelling of atomic rich air in the winter hemisphere (e.g., Rishbeth et al., 2000; Pavlov and Pavlova, 2005). The semiannual anomaly is found to be global and is theoretically suggested to be caused by the variations of the neutral circulation in the thermosphere-ionosphere system which changes the ratio between atomic oxygen and molecular nitrogen concentrations (O/N_2) (Rishbeth et al., 2000). The cause of annual anomaly as suggested by Zeng et al. (2008) is contributed by the displacement of the geomagnetic poles from the geographic poles in addition to the changes in solar EUV radiation and the difference of Sun-Earth distance between December and June as simulated by TIEGCM model. The tides propagating from lower altitudes also contribute to this asymmetry, but to a lesser extent.

As the equatorial ionization anomaly (EIA) is responsible for influencing the most, UHF radio propagation range determinations based on the GPS satellite signals contributes to the enhanced ionospheric scintillation effects produced by the spread F/plasma bubbles irregularities on the trans-ionospheric radio wave propagations during the evening to nighttime (Abdu, 2005). Hence it has become a crucial challenge for the sophisticated models to represent the upper atmosphere in the EIA region (e.g., Huang et al., 1989; Rastogi and Klobuchar, 1990). The International Reference Ionosphere (IRI) is one of the most widely used ionospheric model which is being constantly improved and updated by the scientific committee. After several years of upgradation, the recent version of IRI: IRI-2012 has been released with many enhanced features. As IRI is a data driven model, the accuracy of the model in a specific region and/or time period depends on the availability of reliable data for that specific region and time and hence may also deviate significantly from real observations in regions, for example the equatorial and low-latitude regions (Bilitza and Reinisch, 2008; Bilitza et al., 2014). Hence the validation of IRI is important due to the growing applications in diverse areas of ionospheric investigations with a wide varieties of objectives.

Many previous investigators have compared the observations with the IRI model for validations. Batista and Abdu (2004) using ionosonde observations during low and high solar activity observed highest discrepancy in NmF2 and foF2 during post-sunset and nighttime and in general IRI underestimated hmF2 and over estimated foF2 over the equator. Wang et al. (2009) compared the foF2 and hmF2 ionosonde observations over Hainan (19.5°N, 109.1°E) during 2002–2007 and found that though model follows the trend but under-/over-estimated foF2 from noon/sunrise to sunrise/noon respectively. The IRI-hmF2 was in agreement except over-/under-estimated in day-/night-time in summer in high-/low-solar activity respectively. Some of the recent studies in the Indian sector have also been reported using the GPS measurements (Mukherjee et al., 2010; Aggarwal, 2011; Rathore et al., 2015; Karia et al., 2015). Mukherjee et al. (2010) compared the GPS-TEC with IRI-2001 and observed a higher variability on quiet days as compared to disturbed days throughout the day. Aggarwal (2011) using IRI-2007 found a good agreement of observed and predicted TEC over Rajkot (22.29°N, 70.74°E) during the daytime but underestimation at other times. The predicted TEC by NeQuick and IRI01-corr was found in more agreement to the observed TEC during the daytime whereas during nighttime and morning hours, IRI-2001 exhibited lesser discrepancy in all seasons. Using the latest IRI-2012 model, Karia et al. (2015) found IRI in agreement for the dusk and noon during 2010–2012 but found discrepancy in solar minimum year, 2009 for Surat (21°9′N, 72°47′E) station. Rathore et al. (2015) reported overestimated TEC values by model during the winter of 2012–2013 and attributed it to the foF2 discrepancies in the model over Varanasi (geog. 25°16′N, 82°59′E). As the usage of IRI model is increasing for the prediction of ionospheric behavior (Aggarwal et al., 2009; Aggarwal, 2011; Maltseva et al., 2012; Sharma et al., 2016), for civilian and military applications such as HF communication and ray tracing applications (Azzarone et al., 2012) and for providing corrections to the GPS service providers (Klobuchar, 1986) for the ionospheric delay corrections, hence a comparison of IRI model with the observations and the suggestions for the improvements of the IRI becomes significant. Hence, here the aim of study is to investigate the ionospheric variability in peak electron density (NmF2) and corresponding altitude (hmF2) over the Indian region (Geog. ~5–40°N and 60–100°E) using the satellite-based COSMIC measurements during the solar cycle 24 (April, 2006–December 2013) and suggest the corrections in improving the IRI-2012 model. The hmF2 and NmF2 has been extensively monitored previously by using the ground-based ionosondes at individual sites over Indian regions (e.g., Sharma et al., 1999; Sethi and Mahajan, 2002; Rama Rao et al., 2006; Sethi and Dabas, 2006; Yadav et al., 2010). Here, in Section 2, we describe the data used in the study and followed by the Results and Discussion in Section 3. The summary is presented in Section 4.

2. Data analysis

To examine the background conditions during 2006–2013, the daily solar flux indices: EUV flux and F10.7 and geomagnetic indices: Dst and Ap are obtained from the OMNI website and EUV fluxes from the SEM instrument aboard SOHO satellite (http://www.usc.edu/dept/

space_science/) in 26–34 nm and 0.1–50 nm (Judge et al., 1998) respectively. The F10.7 index (Solar Flux Units, 1 sfu = 10^{-22} W/m^2/Hz, obtained by the OMNI website) is the solar radio emission at the 10.7 cm radio wavelength and was used in past as a proxy for EUV and Lyman-α irradiances (Richards et al., 1994a; Kane, 1992). We considered the solar proxy P = (F10.7 + F10.7A)/2 to represent the solar activity, F10.7A is the average of F10.7 for previous 81-days as suggested by Richards et al. (1994a), Liu et al. (2006) and Brum et al. (2011). Brum et al. (2011) found P a better proxy of solar activity control of hmF2 and foF2 over Arecibo. As the TEC production is mainly in the wavelength 0.1–50 nm EUV band which also produces O^+ (Richards et al., 1994a, 1994b), hence this EUV band is considered a good index for electron production. As the earth's ionosphere strongly responds to strong geomagnetic storms producing major changes in the ionospheric dynamics, structure and chemistry. Hence we restricted our dataset to low geomagnetic activities (daily Ap $\leq$ 20) to investigate the quiet time ionospheric behavior.

2.1. NmF2 and hmF2 from COSMIC

A constellation of six satellites, called the Constellation Observing System for Meteorology, Ionosphere, and Climate (COSMIC or FORMOSAT-3), was launched on 15 April 2006 from Vandenberg Air Force Base, California (Schreiner et al., 2007) from the same rocket and initially followed the same orbit, with all six moving along the same path over 512 km. Then later raised to ~800 km orbit and the individual satellites became 30° apart. Under the assumption of spherical symmetry of ionosphere, the electron density profiles can be retrieved from either the bending angles or the TEC data (computed from the L1 and L2 phase difference) obtained from the GPS occultations (e.g., Hajj and Romans, 1998; Schreiner et al., 1999). This radio occultation (RO) technique has the advantages of limb sounding geometry, global coverage, and high vertical resolution in comparison with traditional ionospheric monitoring methods. The ionospheric profiles are retrieved by using the Abel inversion technique from TEC along LEO–GPS rays (Schreiner et al., 1999; Syndergaard et al., 2006). The considered main source of inversion error is the spherical symmetry approximation. Yue et al. (2010) compared COSMIC Ne profiles with the NeQuick electron density model (using resolution of 50 km for TEC) and found using simulations that the Abel inversion method introduces significant errors in electron densities in the low-latitude region. The spherical symmetry assumption is not satisfied at low latitudes where electron density has strong horizontal gradients whereas errors are relatively small at all altitudes at mid- and high-latitudes. An error analysis showed the absolute (and relative) standard deviations of the differences in the retrieved and true values to be 3.2×10^{10} m^{-3} (16%) and 1.4×10^{11} m^{-3} (15%) for NmF2, and 8.9 km (2%) and 7.4 km (2%) for hmF2 during nighttime and daytime, respectively. This indicated that the retrieved values of NmF2 and hmF2 are in general in good agreement with the true values, but the reliability of the retrieved electron density degraded at the low altitudes. On comparing the COSMIC values with ionosondes, Chu et al. (2010) found that COSMIC-NmF2 are systematically lower than the ionosonde-NmF2 and the discrepancy is smaller in low and mid-latitudes but higher in high-latitude region. Whereas the COSMIC-hmF2 is higher than ionosonde-hmF2 with difference in the two can be as large as 20% or more in equatorial and low-latitude regions. This feature suggests that the inhomogeneous distribution of the electron density along the GPS ray path during the occultation also plays an important role in affecting the correlation between the COSMIC satellite and ground-based ionosonde measurements. Considering these factors, we obtained the COSMIC measurements of second level data provided by CDAAC – "ionprf" files containing information about ionospheric electron density profiles (EDPs) and then obtained the peak electron density (NmF2) and corresponding altitude (hmF2) of the ionospheric F2 layer for each occultation orbit over nearly Indian longitudinal sector (~5–40°N geog. lat. and 60–100° E geog. long.) for each season and year. As our aim is to examine the variability during each season, the daily NmF2 and hmF2 values have been grouped in three seasons: summer, (May, June, July and August), winter (November, December, January and February) and equinox (March, April, September and October) respectively. As the ionospheric behavior is different over equatorial (geog. 5–10°N, geomag 3.5°S–2°N) and low-latitude (geog. 15–30°N, geomag 6–20°N) regions, the data for both the regions are separated.

2.2. NmF2 and hmF2 from International Reference Ionosphere (IRI) model

The study of ionospheric variability has resulted in the improvement and development of various ionospheric models (for e.g. Bent, SLIM, PRISM, SUPIM, NeQuick etc). One of the widely used model based on the data from the network of ground observations and in-situ measurements is the IRI-2012 model (International Reference Ionosphere, http://omniweb.gsfc.nasa.gov/vitmo/iri2012_vitmo.html), which is the latest version of IRI. IRI is an international project sponsored by the Committee on Space Research (COSPAR) and the International union on Radio Science (URSI) and is being improved and updated regularly. Since its first establishment in 1978, the IRI has undergone regular revisions to improve its prediction capabilities (Rawer et al., 1978; Bilitza, 2001, 2014; Bilitza and Reinisch, 2008). A brief history of the IRI project and description of the latest version of the model (IRI-2012) is recently reported in Bilitza et al. (2014). The IRI provides averaged behavior of ionospheric electron density, electron content, electron and ion temperatures, and ion composition as a function of height, location, local time, and sunspot number. The major data sources of IRI are the worldwide network of ionosondes, the powerful incoherent scatter radars (Jicamarca, Arecibo, Millstone Hill, Malvern, St. Santin), the ISIS and Alouette topside sounders, and in-situ instruments on several satellites and rockets.

The two key parameters used to generate the ionospheric electron density profile in IRI are the critical frequency (foF2) and hmF2 of F-layer respectively. The IRI model uses two different computer programs as subroutine to predict the foF2 and hmF2/M(3000)F2 based on the 12-month running average of the sunspot number (Rz12): (1) CCIR model: developed by the International Radio Consultative Committee (CCIR) in 1966 and (2) URSI model: developed by Rush et al. (1989) and both models uses a similar spherical-harmonics-type representation. The CCIR model is based on monthly median values of foF2, hmF2 and M(3000)F2 obtained by the worldwide network of ionosondes (150 stations) during the years 1954–1958 (using ~10,000 station-months of data) and is first represented by a Fourier time series with coefficients applied to a special form of Legendre functions (in geodetic latitude, longitude and modified dip latitude). This model has shortcomings above the oceans and in the southern hemisphere, where ionosonde measurements do not exist or are sparse and there the aeronomic theory is used to fill the data gaps before applying the spherical harmonics mapping procedure. Hence CCIR option is recommended for continental areas, while the URSI option outperforms the CCIR option over the ocean areas. The URSI coefficients are based on over 45,000 station-months of ionosonde data (about 180 stations worldwide). The shortcoming of URSI is that the theoretical model was adjusted such that it agreed with measured foF2 values over land, and then was used to compute screen points in data sparse regions. To obtain the seasonal behavior of NmF2 and hmF2, we run the IRI-model for all months by incorporating the daily and 81-day F10.7 indices for each month using both CCIR and URSI options for the F peak model for geographic equatorial (0°N) and low-latitude (20°N) and 77°E longitude, obtained the NmF2 using relation with foF2: ($NmF2(m^{-3}) = 1.24 * 10^{10} * (foF2)^2$, foF2 in MHz) and then combined months as also obtained for COSMIC measurements for seasonal behavior. The model provides three options for bottomside thicknesses (Bil-2000, Gul-1987, and ABT-2009) and we used ATB-2009 to compute the electron density profiles.

3. Results and discussion

3.1. Background conditions during study period (2006–2013)

Fig. 1 represents the background variability of daily solar flux (F10.7 and F10.7P), EUV fluxes in 0.1–50 and 26–34 nm wavelengths and geomagnetic indices (Dst and Ap) after the launch of COSMIC from 22 April 2006 to 31 December 2013 mission period respectively. The daily F10.7 and F10.7P (Fig. 1(a)) varied from ~65 sfu to ~191 sfu during the period and increased from year 2008 to 2013 exhibiting higher solar activity in 2012–2013. The day-to-day variability of solar flux is also higher (annual standard deviation, stdev ~ 18–25 sfu) during 2011–2013 whereas during low solar activity (LSA) period, higher variability (stdev ~ 2–4 sfu) is observed in 2006 to mid 2008 whereas the variability is almost negligible during mid-2008 to mid-2009 year (stdev ~ 1–2 sfu) respectively. We divided the whole solar activity period as A (LOW) (2006–2007, yearly averaged F10.7 (avF10.7): 76 sfu), B (MIN) (2008–2009, avF10.7: 70 sfu), C (MOD) (2010–2011, avF10.7: 96 sfu) and D (MAX) (2012–2013, avF10.7: 121 sfu) representing the low, minimum, moderate and maximum phases of solar activity respectively based on F10.7 for a relative comparison. Similar to F10.7, the EUV fluxes (Fig. 1(b)) in both wavelengths also follows the same trend except for a few days when higher values of EUV fluxes are observed which occurs during the solar flare occurrence when the EUV emission enhances from the Sun. The Ap values are higher and Dst lower (Fig. 1(c)) on a few days representing the occurrence of a few moderate storms during the period (Dst minimum up to ~−116 nT and Ap maximum to 94). The horizontal line represents the demarcation line of quiet days and disturbed days when Ap ~ 20, the days above this line are not considered in further study. Fig. 1(d) and (e) represents the variability of F10.7P and EUV flux in 0.1–50 nm for quiet days ($Ap \leq 20$) during each phase of solar activity for each season. The similar trend is followed in both F10.7 and EUV fluxes in all seasons with lowest values in MIN phase and maximum in MAX phase of solar activity. Both F10.7 and EUV flux for each season in LOW, MIN and MAX phase (F10.7: A ~ 77 sfu, B ~ 70 sfu and D ~ 121 sfu) are same whereas for MOD phase, the F10.7 and EUV is lower in summer (F10.7 ~ 92 sfu, EUV $\sim 2.4 \times 10^{10}$ ph/cm^2/s) than other seasons (F10.7 ~ 100, EUV $\sim 2.6 \times 10^{10}$ ph/cm^2/s) respectively.

3.2. Diurnal variability of NmF2 during seasons

To examine the day-to-day variability of NmF2 and hmF2 in each season over both equatorial and low-latitude regions, the hourly mean, median (med), standard deviation (stdev), upper quartile (UQ) and lower quartile (LQ) are obtained using the daily values. To estimate the variability, variability index (VI%) and relative variability (RV%) are obtained and defined as the percentage deviations of UQ and LQ and the standard deviation (stdev) with respect to the median respectively. The range of LQ and UQ covers 50% of all data points and are less affected by the larger deviations, hence are considered a better measure than stdev. Whereas the stdev is a good measure for describing the average deviation from the mean, provided the scatter values do not lies far from the average values and is not a good parameter to interpret in terms of probability. Hence mathematically,

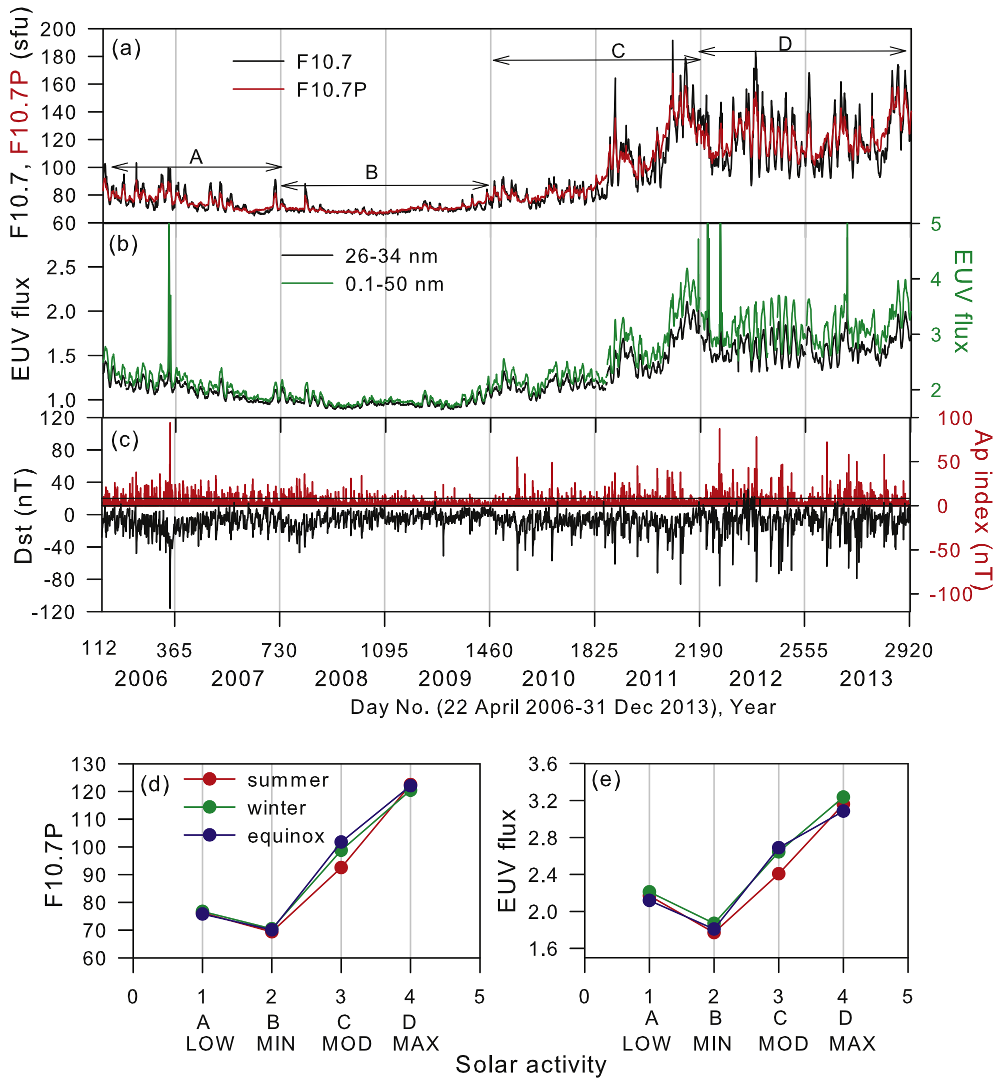

Fig. 1. Variation of (a) F10.7 and F10.7P, (b) EUV fluxes (26–34 and 0.1–50 nm), (c) Ap and Dst indices during the complete period (April, 2006–Dec 2013) respectively. The A, B, C and D represents the low (2006–2007), minimum (2008–2009), moderate (2010–2011) and maximum (2012–2013) solar activity phases. The horizontal line represents the Ap = 20 nT. Last panel represents the yearly averaged variation of solar indices ((d) F10.7P and (e) EUV, 0.1–50 nm) during quiet days of each season. Note: 1 EUV flux = 1×10^{10} ph/cm^2/s.

$$VI(\%) = \frac{(UQ - LQ)}{med} * 100 \quad \text{(a)}$$

and

$$RV(\%) = \frac{stdev * 100}{med} \quad \text{(b)}$$

The first row in each panel of Fig. 2 represents the diurnal behavior of hourly mean of NmF2 (line with symbol) with deviations: NmF2 + stdev and NmF2-stdev (symbols) over equatorial and low-latitude regions during each phase of solar activity for all three seasons: (a) summer, (b) winter and (c) equinox respectively. The NmF2 is minimum throughout the nighttime, start increasing in early morning hours when the photoelectron production begins and attains a maximum during noontime and then decreases in the evening due to the competitive effects of absence of photo-ionization and recombination of electrons with neutrals and ions. We found that as the solar activity increases, the mean NmF2 also increases throughout the day, with higher rise in noontime (from 65×10^4 cm^{-3} to 200×10^4 cm^{-3}) than nighttime (from 5×10^4 to 120×10^4 cm^{-3}) in all seasons respectively. The difference over equatorial and low-latitudes in nighttime NmF2 is almost negligible in summer for all solar activities and also for winter and equinox but not in the MOD and MAX activity when the NmF2 values are higher over equatorial region. Whereas the difference in noontime NmF2 over equatorial and low latitude is negligible in both summer and winter during LOW and MIN solar activity but is higher (up to 30×10^4 cm^{-3}) during MOD and MAX solar activity periods. Whereas during equinox, the noontime NmF2 is higher over the low-latitudes for all solar activities and the difference of equatorial and low-latitude NmF2 increases (30×10^4 cm^{-3}–40×10^4 cm^{-3}) with increase in

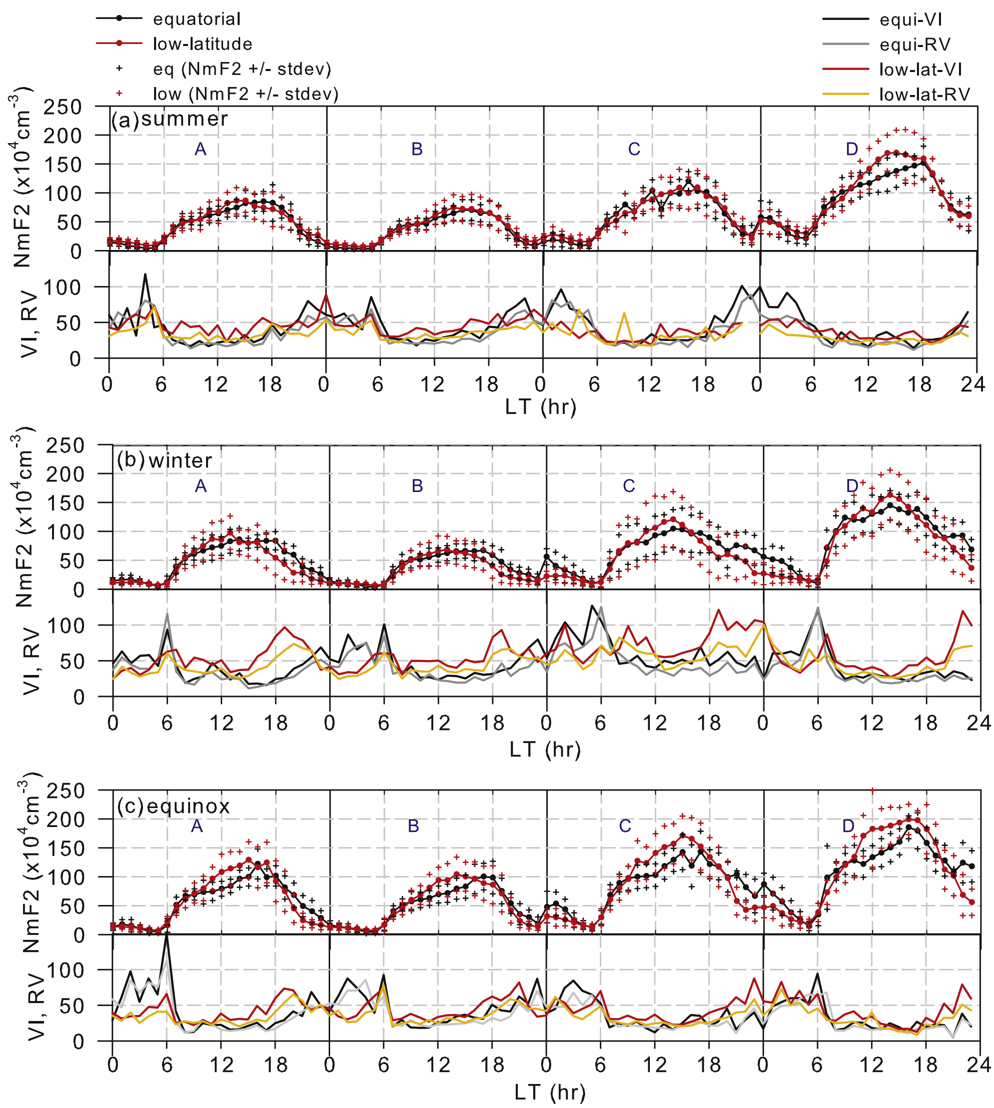

Fig. 2. Upper row in each panel represents the diurnal variation of hourly mean NmF2 (line + symbol) and deviations (NmF2 + stdev and NmF2-stdev, symbol) and the second row shows the hourly percentage of variability index (VI) and relative variability (RV) during (a) summer, (b) winter and (c) equinox over equatorial and low-latitude and solar-activity phase respectively. Unit for deviation is $\times 10^4$ cm^{-3} respectively.

the solar activity and indicates an existence of stronger EIA in summer and winter during MOD and MAX solar activity and during all solar activity periods in the equinoxes respectively. A strong evening enhancement (~1800 LT) is observed over both the latitudes during MOD in winter and over equator in equinoxes during all levels of solar activity. The post-midnight enhancement in NmF2 is only observed (for both regions) during MOD and MAX solar activity where the strength increases with the increase in solar activity (higher in winter and equinox) respectively.

The hourly stdev in NmF2 representing the day-to-day variability for each season is lower during nighttime but higher during noontime when the mean values are also higher. The lower stdev is observed in noontime during low solar activity (LOW and MIN, $<25–30 \times 10^4$ cm^{-3}) and is highest during MOD and MAX in winter and equinox over low-latitude (up to 65×10^4 cm^{-3}) and during post-midnight period of MIN and MOD (up to 28×10^4 cm^{-3}) respectively. The day-to-day variability in NmF2 may be attributed to the changes in the EUV flux, equatorial electrojet (EEJ) and dynamics of the neutral winds (Rama Rao et al., 2006).

The bottom rows in each plot of Fig. 2 representing VI and RV in NmF2 is lower (<50%) over both regions during noontime in all seasons. Over equator, the VI and RV is higher up to 150% in early morning, whereas over low-latitude, the deviation is higher during morning hours as well as nighttime (up to ~100%) respectively. We found a higher variability (VI and RV) in LOW and MIN activity period. Similar higher variability in TEC over Indian low-latitude region is observed by Aggarwal (2011) during nighttime and morning hours than during daytime (their Fig. 1) in all months during low solar activity period (2005–2006). Ezquer and Mosert (2007) for American and European sector also found a higher variability in foF2 during low solar activity than in high solar activity, and was larger by night than by day similar to our observations. Sethi et al. (2007) over Indian low latitude region also found lower variability index (VI) in general during daytime hours than nighttime during high solar activity for all the seasons, while during low solar activity, VI of foF2 exhibited irregular diurnal pattern (~20–45%) during all seasons. They also found a solar activity dependence of VI with maximum values during periods of low solar activity in all seasons except for winter during pre-dawn and post-sunset hours.

3.3. Diurnal variability of hmF2 during seasons

Another significant ionospheric parameter, *hm*F2 provides useful information from which the meridional winds may be deduced for understanding the ionospheric behavior and assessing the thermospheric general circulation models (e.g. Miller et al., 1986, 1997). Similar to NmF2, the diurnal variability of hmF2 over both the latitudinal regions is obtained during different solar activity and seasons as represented in Fig. 3. The diurnal trend of hmF2 is similar over both latitude and exhibits two maxima (evening-midnight and noontime) and two minima (sunrise and sunset) in each phase of solar activity with higher values over the equator throughout the day in general irrespective of season and solar activity. In general, F region electrodynamic plasma drifts are upward and westward during the day and downward and eastward at night and have largest amplitudes around 0900 and 1100 LT with typical values of 25–30 m/s (Scherliess and Fejer, 1999). From Fig. 3 for all seasons, the hmF2 rises gradually from ~0700 LT onwards, and a noontime peak occurs around 1400 LT over both latitudes; however, the noontime peak is much lower than midnight values over low-latitude in winter. Thereafter over the low latitude, the hmF2 decreases and becomes lowest around 1800–1900 LT for each season. We found using COSMIC observations that the noontime hmF2 varied from 310 km to 415 km and 235 km to 350 km over the equatorial and low-latitude regions respectively. Whereas the hmF2 varied from 230 km to 415 over equator and 220 km to 340 km over the low-latitude regions throughout the period. This is lower as found by Rama Rao et al. (2006) using ground ionosonde observations for a very high solar activity (cycle: 23) year of 2001 (F10.7 ~ 181) over Indian region, hpF2 (~hmF2) varied from ~275 km to 575 km at the equatorial region and 300 km to 350 km at and near the anomaly crest regions throughout the day. They also found a higher variability over an equatorial station (Trivandrum) in December 2001 with daytime peak as high as 575 km and this was expected as the EEJ is stronger in the winter months compared to the summer months, consequently, the F-region gets elevated to higher altitudes at the equator due to the increased $E \times B$ drift. In agreement to the Ionosonde observations over Indian region, using our COSMIC observations, we also found a higher noontime peak (~320 km) over the equator than low-latitude (~250 km) in winter in 2006–2007 which increases over both the latitudes (~365 km over equator and ~300 km over low-latitude) with increase in solar activity (2012–2013) respectively.

We found similar hmF2 (~230 km) during early morning (0600 LT) in all seasons except being higher in MOD and MAX solar activity periods (Fig. 3). Another diurnal peak in hmF2 over equator is observed in evening (1800–2000 LT) in winter and equinox which increases with the solar activity. This is consistent with the observed NmF2 increase in MOD and MAX activity (Fig. 2). The NmF2 at the equatorial region is higher in winter and equinox in MOD (1800–2400 LT) and MAX (0000–0600 LT). This increase in winter and equinox is the post-sunset enhancement and post-midnight enhancement in NmF2 which is consistent with the rise in hmF2 over equator (Fig. 3 (b) and (c)) where the plasma gets lifted up to higher altitude where loss rate by recombination is less resulting in the higher electron density. And this decreased slowly in the post-midnight hours hence higher NmF2 over equator in 0000–0600 LT respectively. During daytime, as the temperature increases, the concentration of atomic oxygen and loss coefficient, which is proportional to the molecular components, both increase, resulting in higher altitudes of layer maximum; accordingly, the increase of hmF2 from morning to afternoon is due to an increase in the temperatures (Sethi et al., 2004). Around the dusk time, there is an enhancement in the vertical drift of the F layer plasma, produced by an enhancement in the zonal electric field, known as the pre-reversal enhancement (PRE) of electric field. Over equator, the magnitude of uplift of F-layer in evening-time is observed more clear during MOD and MAX solar activity whereas over low-latitudes, the midnight hmF2 is found which is even higher than noontime in all seasons and years. In the evening, as the rate of ion production decreases, an upward drift causes an additional uplift of the layer produced by a change in the direction of the thermospheric winds and hence increases the hmF2. The drift rate increases toward midnight, causing a further rise in the F2-layer around midnight. The F2 region attains a maximum height around midnight caused by an increase of the upward drifts produced by the meridional winds in the neutral air (Hanson and Patterson, 1964; Kohl and King, 1967) whereas around sunrise hours, with the beginning of intensive ionization, the electron concentration near the F2-peak increases at a rate which depends primarily upon the production rate, and thus, the layer maximum shifts downwards due to rapid production of ionization in the lower F-region (see, e.g. Rishbeth and Garriot, 1969).

The variability represented by stdev ranged between 15 km and 70 km throughout the period over both regions and seasons respectively. The VI and RV of hmF2 (Fig. 3) represented in the bottom rows of each panel for equator represents lower values (<20%) in seasons throughout the day except the morning hours when both variabilities are

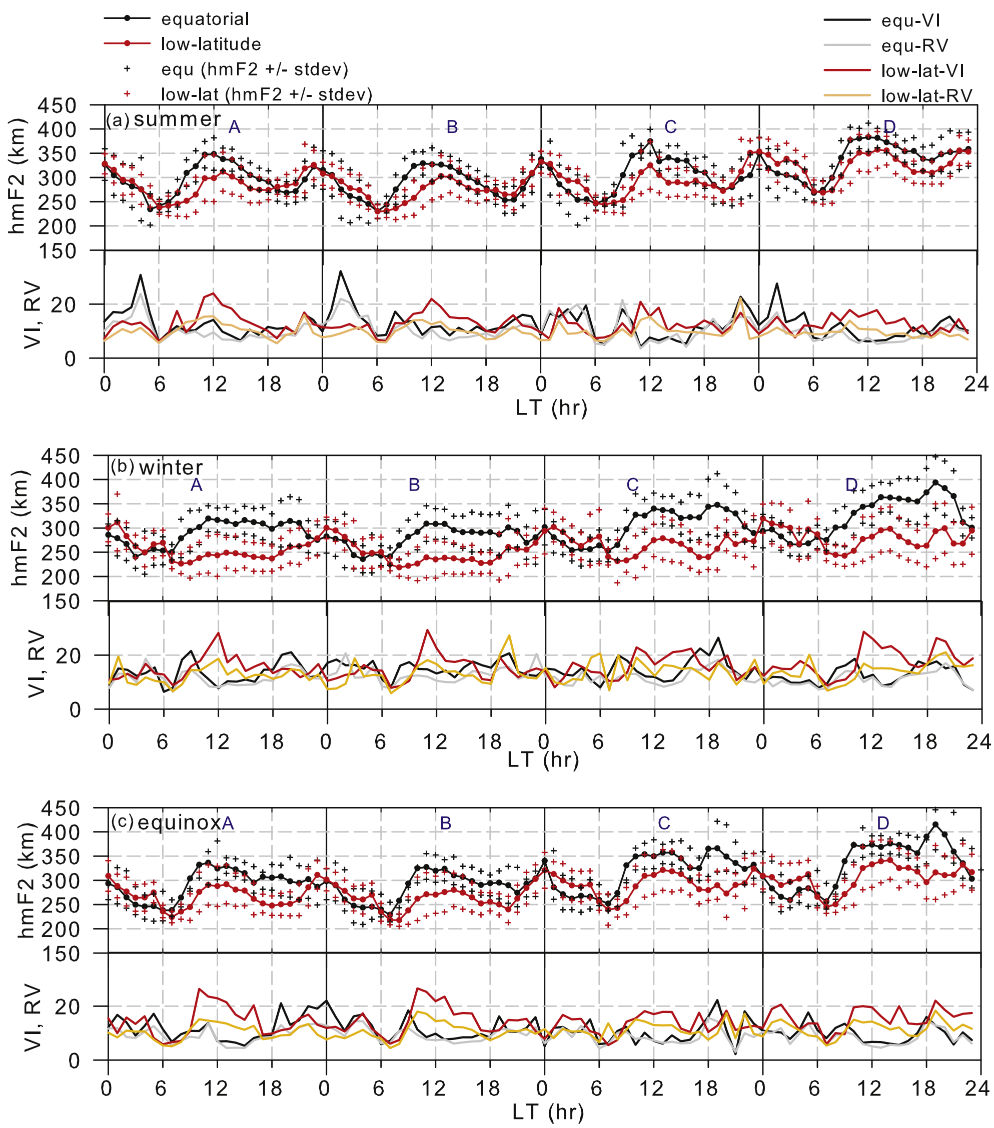

Fig. 3. Same as Fig. 2 but for hmF2. The unit of dev is km respectively.

a little higher (30%) in summer. Whereas over low-latitude, the variabilities are higher (VI ~ 30% and 25%) during noontime in all seasons and the VI decreases with the rise in solar activity. This higher variability is in agreement with Sethi et al. (2004). Sethi et al. (2004) using ionosonde at Delhi (28.6°N, 77.2°E) also found a large diurnal and day-to-day variability in hmF2 during all seasons, with higher values around midnight than by day and higher variability during the nighttime (~225–475 km). They also observed an earlier diurnal peak in summer (1000 LT) respectively.

3.4. Comparison of NmF2 with IRI 2012 model

The observed NmF2 and hmF2 by COSMIC measurements are compared with IRI-2012 model for each season and different phases of solar activity over both equatorial and low-latitude to validate its predictability. Figs. 4 and 5 are obtained from the hourly means of observed and modeled NmF2 and hmF2 respectively using both options available in IRI-2012: CCIR and URSI coefficients for each season. For a quantitative assessment of IRI model, the relative percentage deviation (RPD) between the observed and predicted values for a given parameter is defined as:

$$RPD = \frac{(Xo - Xi)}{Xo} \times 100 \qquad \text{(c)}$$

where Xo denotes the observed values and Xi the modeled value for NmF2 or hmF2 using either the CCIR or URSI coefficients respectively.

The diurnal variability of observed NmF2 for each season is represented in first row of Fig. 4 for equatorial (left panel) and low-latitude (right panel) respectively. The observed NmF2 shows a clear solar activity dependence and increases with the increase in solar activity throughout the day at both latitudes. Over the equatorial region, the

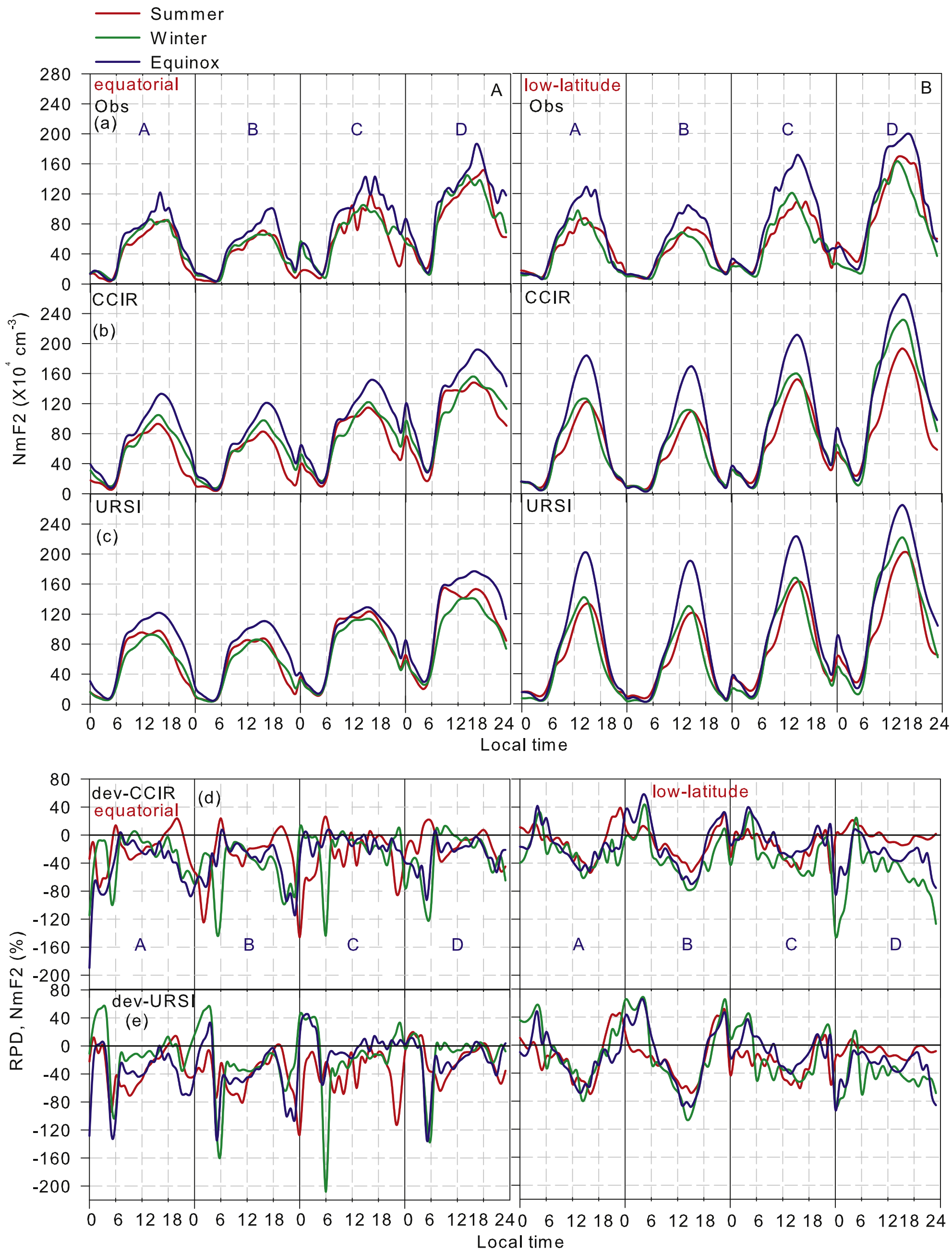

Fig. 4. Represents the diurnal variability of hourly mean NmF2 using (a) observations, (b) CCIR option and (c) URSI option during all three seasons over equatorial (left-column) and low-latitude (right-column) respectively. The last two rows shows the hourly relative percent deviation (RPD) of modeled and observed NmF2 using (d) CCIR and (e) URSI options for each season and both latitudes respectively. Note: The positive (negative) values of RPD indicates lower (higher) estimation of NmF2 by IRI model.

noontime winter anomaly is absent during LOW and MIN and is weaker during MOD and MAX phase whereas over low-latitude, winter anomaly is stronger in LOW and MOD but absent in MIN and MAX (B and D) phase of solar activity respectively. The winter anomaly over Indian equatorial region was previously reported by Rama Rao et al. (2006) using GPS-TEC during low solar activity (2004–2005, F10.7 ~ 99 sfu) and Sripathi (2012) using COSMIC observations during year 2008 (F10.7 ~ 69 sfu) and Batista and Abdu (2004) over African equatorial regions for both low (~72 sfu) and high solar activity (~170 sfu) respectively. Our observations of the absence of winter anomaly in NmF2 during MIN over low-latitude is in agreement with the TEC observations as observed by Chauhan and Singh (2010) and Aggarwal et al. (2012). The presence of winter anomaly in MOD (C) phase of activity over equatorial and low-latitude is attributed to the lower F10.7 and EUV flux in summer than winter (Fig. 1(d) and (e)) which would contribute to the lower production of electrons in summer respectively.

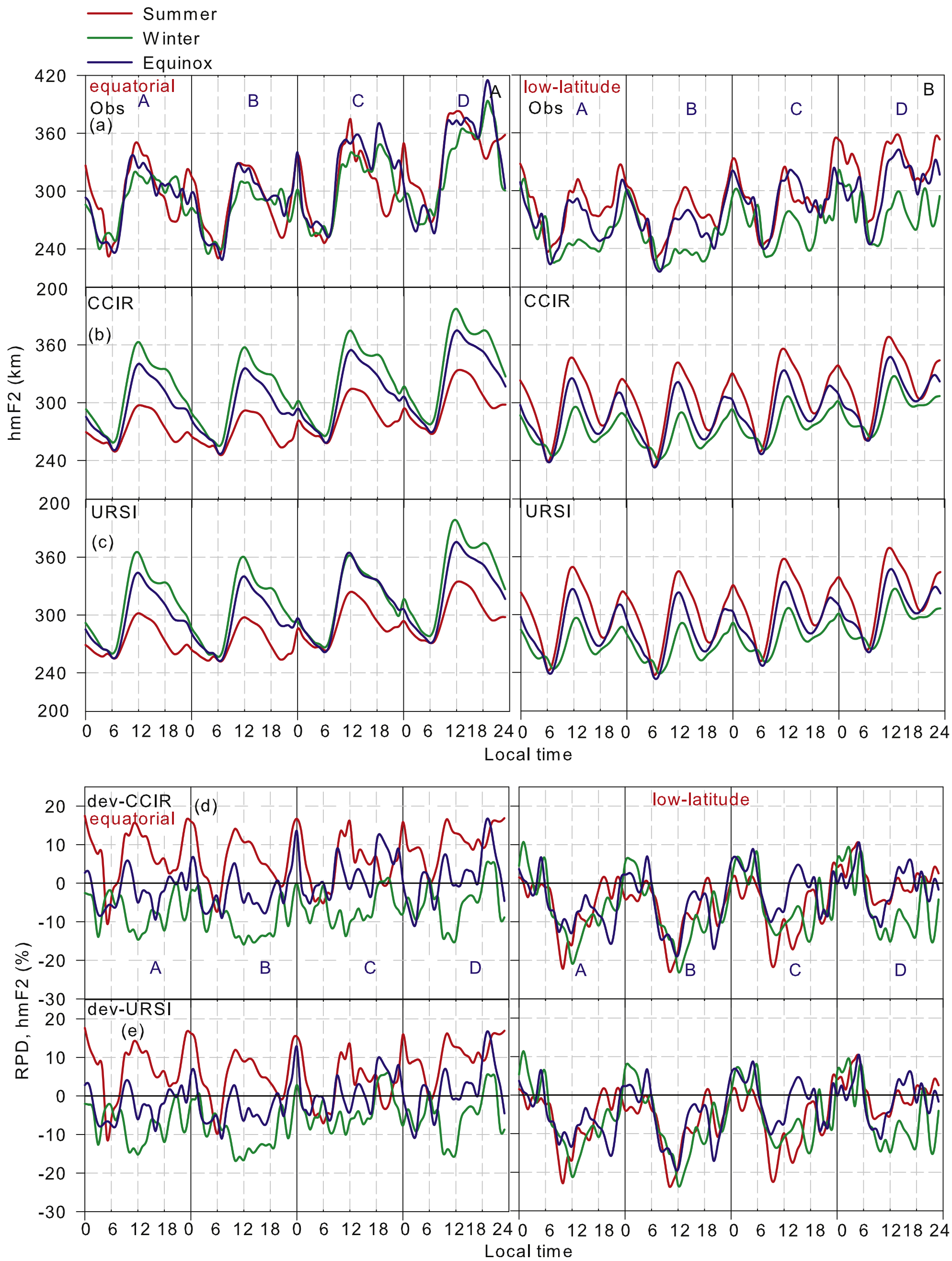

Fig. 5. Same as Fig. 4 but for hmF2.

The various other factors contributing to the electron density distributions other than EUV flux are the sub-solar point, O/N_2, thermospheric winds, EEJ respectively which may be responsible for the winter anomaly in LOW activity over low-latitude. Aggarwal et al. (2012) using TEC over Indian region showed higher correlation of magnitude of peak TEC at anomaly region (crest, Ic) with the solar flux and EEJ during summer than winter compared to other factors (their Fig. 5b). Rishbeth and Garriot (1969) and Walker (1971) reported the winter anomaly of daytime peak at low-latitude mainly occurring during medium and high solar activity periods caused by the seasonal changes in the neutral gas compositions. The vertical winds are downward (upward) in the winter (summer) hemisphere resulting in increase (decrease) of the O/N_2 ratio. Higher O/N_2 ratio means more production of ionization and lower loss rate of electrons. Consequently, recombination gets weaker in the winter hemisphere, leading to higher electron densities in the winter than summer solstice and hence the winter anomaly occurs. Further, the **effective loss rate values tend to be greatest in the winter at sunspot minimum but toward a maximum a reversal takes place and then the greatest loss occur in the summer.** Our results for Indian region over low-latitude exhibits winter anomaly over low-latitude stronger in the LOW and MOD solar activity but absent in MIN and MAX solar activity indicating the role of other factors also in electron density distribution like O/N_2, EEJ and thermospheric winds. During the equinoxes, the subsolar point gets closer to the equator, where the eastward electrojet and the associated electric field is also often stronger. As the photo-electron production is higher and stronger eastward electric field exists in equinoxes hence the fountain effect would be strong. Whereas during the solstices, photoelectrons at the equator decreases as the subsolar point moves to higher latitudes and the fountain effect is expected to wane (Wu et al., 2004).

Our results in Fig. 4 represents semi-annual anomaly in all phases over both regions and is stronger over low-latitudes. As the F-region ionosphere is electro-dynamically coupled with the E-region ionosphere, the semi-annual variability of amplitude of diurnal tide in lower thermosphere may induce the semi-annual variation of the E-region EEJ and hence affects the F-region plasma drift. As the EEJ currents are stronger in equinoxes, hence more ionization is uplifted from the equator and transferred to the crest latitudes. As the solar EUV input is also high over ionosphere during equinoxes, it causes a strong upwelling by day accompanied by poleward winds, ultimately balanced by a similar strong down-welling by night accompanied by equatorward winds. The density variations of O and N_2 also exhibits two maximums per year in March and September producing the semi-annual variations. In equinoxes, meridional winds flow toward the pole from the equatorial region which also result a higher NmF2 over the crest regions (Bramley and Margaret, 1968). No seasonal variations in NmF2 during mid-night (0000–0500 LT) is observed in our observations.

In Fig. 4, the second and third rows represents the modeled NmF2 obtained by CCIR and URSI options in IRI. The general diurnal trend of modeled NmF2 is similar to the observations: NmF2 increasing with sunrise (around 0600 LT) and becomes maximum around noontime (1300–1600 LT), decreases to minimum in nighttime and increases again during sunrise hours (0500–0600 LT). The modeled NmF2 also exhibits semi-annual anomaly and solar activity dependence. A weaker winter anomaly is observed during noontime by CCIR-NmF2 for both regions and by URSI-NmF2, only over low-latitude regions respectively during all phases of solar activity. The observed NmF2 (first row in Fig. 4) exhibits the mid-night enhancement during MIN to MAX solar activity during all seasons and latitudes which is also well-modeled by the IRI using both options (Fig. 4(b) and (c)) respectively.

To assess the model quantitatively, the RPD of CCIR and URSI NmF2 from observed NmF2 are obtained as shown in the last two rows of Fig. 4(d) and (e) respectively. The positive (negative) values of RPD defines the under (over) estimation of the modeled values from the observed ones respectively. Over equator, both models overestimates the noontime NmF2 (up to 40% by CCIR, 80% by URSI) respectively. The CCIR model during morning hours, overestimates (up to 150% in winter) but underestimates for other seasons (up to 30%) except the equinoxes during MAX where it overestimates. During nighttime, CCIR overestimates in summer (up to 140%) and up to 100% in other seasons. Whereas by URSI is under-/over-estimated before (0000–0400 LT, up to ~55%)/during (~0600 LT, up to 200%) morning hours respectively. Both models overestimates nighttime NmF2 in all seasons (CCIR: in winter and equinox (80%), summer (150%) and URSI: up to 120%). For low-latitude, similar to equator both models also overestimate noontime NmF2 (CCIR: up to 60%, URSI: 100%) respectively. In conclusion, during noontime the modeled NmF2 seems to be more in agreement by CCIR with overestimation by ~60% as compared to URSI (overestimated by ~90%) in general for both equatorial and low-latitude regions. The discrepancy is higher during nighttime and morning for equator whereas higher discrepancy exists throughout the day for low-latitude. Sobral et al. (2003) found IRI in agreement with foF2 ionosonde observations, although the model appeared to overestimate in August for both years of 1978 and 2000. In further study, they found a difference in shape of electron density profiles obtained by rocket flights in the Brazilian equatorial region and IRI profile at high altitudes. Chuo and Lee (2008) using foF2 observations for year 1994–1999 over Chung-Li (24.90°N, 121.10°E), found a good agreement during daytime by both CCIR and URSI in the IRI-2001 model, but overestimated in nighttime (5% to 80%) and afternoon hours (2–17%) especially during summer. We also found using both coefficients in IRI, the predictions follow well the general trend during seasons. Zhang et al. (2007) using foF2 values over Hainan (19.4° N, 109.0°E) found that both options in IRI systematically underestimates during most time of day (~5% and ~25%), whereas the IRI overestimates (up to ~30%) around pre-sunrise period. They found best agreement in summer by URSI coefficients (±10%). We also found the best agreement in summer solstice but by using both the options during high solar activity. Using Chumphon (10.72°N, 99.37° E, dip 3.22) data for low solar activity period, Wichaipanich et al. (2010) found better estimates in year 2005 and 2006 than 2004 for both the models. They found underestimation during pre-sunrise hours similar to our results (Fig. 4) and concluded that though both options of the IRI overall gave closer foF2 values to observations, but the CCIR results produced better agreement and smaller range of deviation than the URSI results. Our results are in agreement to their findings for both the latitudinal regions.

3.5. Comparison of hmF2 with IRI 2012 model

Similar to NmF2, the variability of observed and modeled hmF2 (by both models) is examined in Fig. 5. The modeled hmF2 exhibited similar diurnal trend to the observed hmF2, however the discrepancy exists in the seasonal variabilities. On comparing the observed hmF2 for different seasons over the equator, the evening enhancement occurs during evening (~1900 LT) in winter and equinox called as PRE and increases with the increase in solar activity. No seasonal difference is observed during morning hours (0600–1000 LT) similar to NmF2. The noontime hmF2 is highest in summer and shows a solar activity dependence over both latitudes. The (b) and (c) in Fig. 5 represents hmF2 by the models (URSI gives higher hmF2 most of time) and exhibits a seasonal difference with the observed hmF2. The last two-rows ((d) and (e)) representing RPD (Fig. 5) exhibiting smaller discrepancies (<20%) throughout the day over both the latitude. Over the equator, the model under-/over-estimates (~15%) most time of day (higher in noontime and morning) in summer/winter but overestimates in morning (10%) respectively with lesser discrepancy in equinox. Whereas for low-latitudes, the discrepancy is similar in all seasons (lesser in morning, 10% but overestimated at other times of day, up to 20%). The hmF2 using CCIR and URSI shows similar hmF2 without much difference. Sethi et al. (2004) using the ionosonde data of Delhi (28.6°N, 77.2°E) and IRI-2001 found lesser deviation (<10%) in 0600–1800 LT while slightly higher (~10–15%) at other times in summer solstice respectively. During winter and equinox, the discrepancies were slightly higher (15–25%) around pre-sunrise (0500 LT) and in afternoon (1400–1800 LT) but matched well in the nighttime (<10%).

3.6. Regression analysis

To exemplify the predictability of IRI-2012 model, hourly observed and modeled NmF2 values (by CCIR ((a) and (c)) and URSI ((b) and (d))) for a complete study period and for each season is plotted without any local time and solar activity selection as represented in Fig. 6. The linear least square fitting ($y = a_0 + bx$, where x and y are the fitted observed and expected modeled NmF2 by IRI using either CCIR or URSI coefficients, b is the slope of the fitted line and a the intercept of the fitted line) and the correlation coefficients (r^2) are shown in each panel. From Fig. 6, we found a higher correlation of modeled with observed NmF2 for both equatorial and low-latitude, but the correlation by CCIR model (r^2) = 0.93 and 0.94) is slightly better than URSI (0.90 and 0.93) for the whole data and each season. The modeled NmF2 by both models are overestimated over equator (4.5×10^4 cm^{-3}–11×10^4 cm^{-3}) but underestimated over low-latitude (1.8×10^4 cm^{-3}–6.5×10^4 cm^{-3}) in different seasons respectively. In conclusion, by regression analysis also we found the CCIR is slightly in more agreement than URSI as both models exhibits similar correlation with the observed values for equatorial-low latitudes. This is also in agreement with the results of Aggarwal (2011) using TEC measurements over an anomaly station in the Indian sector.

Similar to Fig. 6, Fig. 7 is obtained for hmF2 values. Though the modeled hmF2 shows lesser discrepancy with

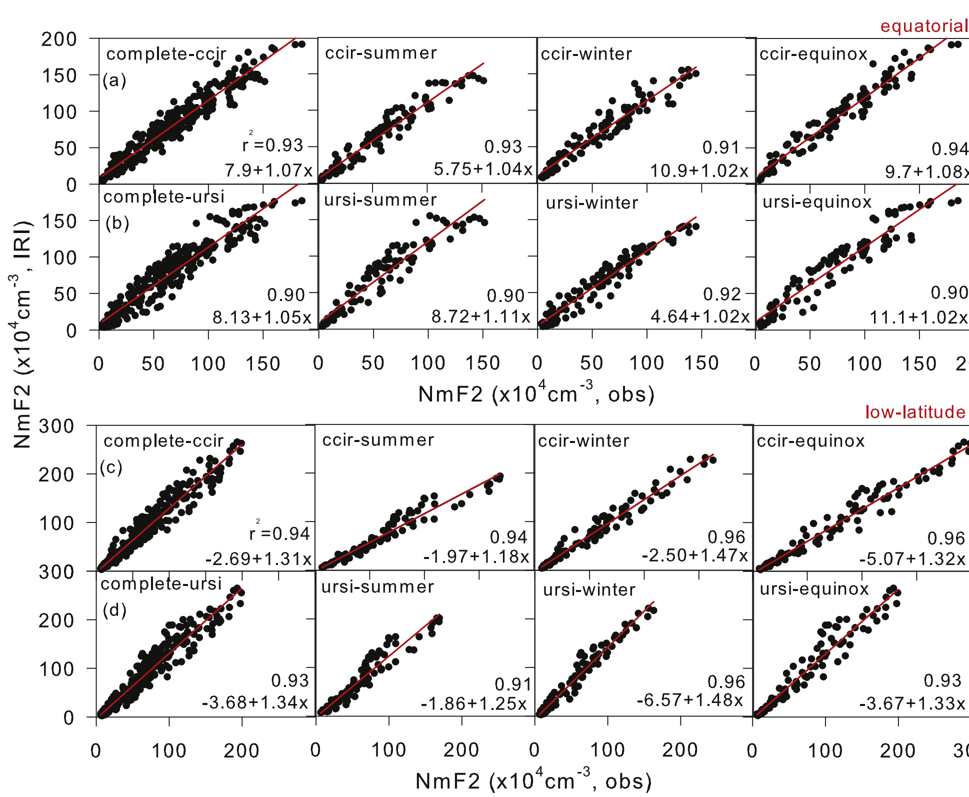

Fig. 6. Comparison of observed NmF2 with predicted by IRI-2012 using CCIR (a and c) and URSI (b and d) options for equatorial (first two rows) and low-latitude (last two rows) during complete study period (first column), summer (second-column), winter (third-column) and equinoxes (fourth-column) respectively. The regression line with correlation coefficient (r^2) is also shown.

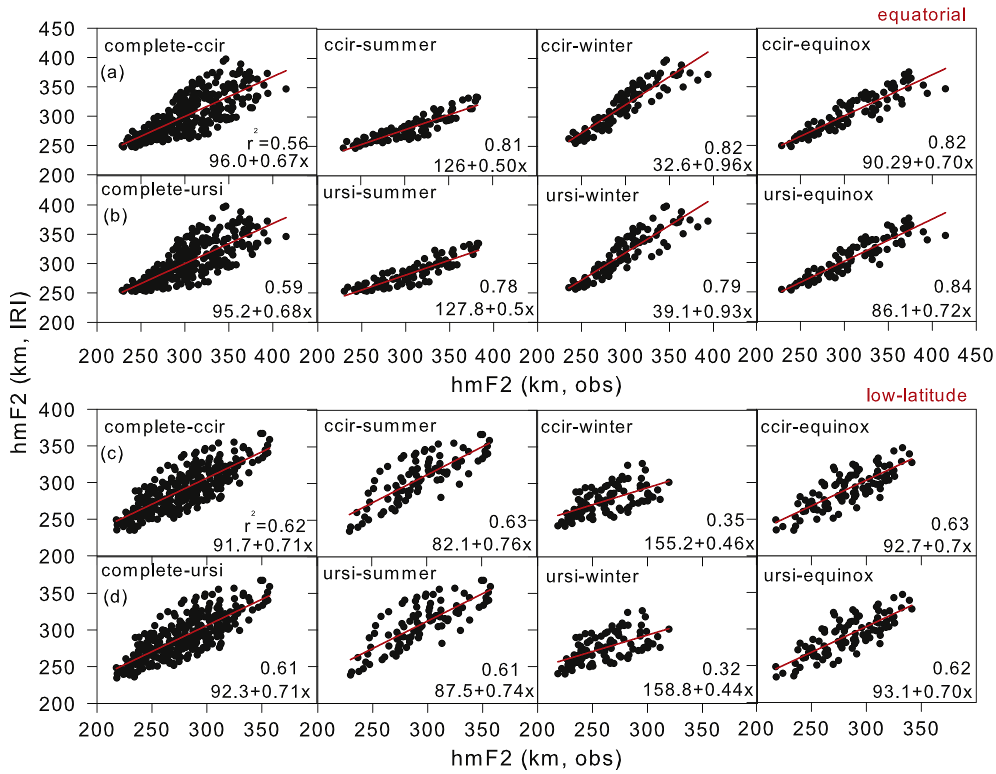

Fig. 7. Same as Fig. 6 but for hmF2 respectively.

observations for some local time of day (Fig. 5) but the correlation is moderate. The over-all correlation is moderate for complete data set by both the models and over the latitudes (~0.56–0.62) respectively with overestimation of predicted hmF2 values up to ~96 km. Over equator, the correlation of observed and predicted hmF2 is strong (~0.78–0.84) for seasons with overestimated values by ~126 km, ~40 km and 90 km in summer, winter and equinox respectively. Though the correlation among the seasons are strong but still correlation is moderate for complete data-set, the reason being that the slope for each season is different and though the IRI follows the trend of observed hmF2 but quantitative differences do exists for each season. Over low-latitude, the correlation is moderate (~0.63) for summer and equinox and weaker (~0.35) in winter by both models with overestimation up to ~85, 92 km and ~155 km respectively. On carefully seeing the hmF2 during winter season using both the models, we found a poor correlation (0.3) of predicted and observed values during the nighttime (2000–0300 LT, not shown as separate figure) which must have contributed to the weaker correlations in the winter solstice. Zhang et al. (2007) also found that earlier version, IRI-2001 using CCIR option also exhibited poor agreement during the nighttime and suggested the corrections needed in the M(3000)F2 values for the ionosonde observations at Hainan (19.4°N, 109.0° E). We found that both models overestimated hmF2 over both the latitudes which is even slightly higher for the low-latitudes. Karami et al. (2011) found a good prediction of NmF2 and hmF2 over Tehran region using IRI-2007 and IRI-2001 model during low solar activity. In addition, their study showed the predictions of IRI-2007 model closer by CCIR coefficients (difference <10% and 20%) to the observations which is in agreement to our observations by IRI 2012 model.

4. Summary

The present study examined the diurnal behavior of significant ionospheric parameters: NmF2 and hmF2 in seasons during different solar activity phases as obtained first time by the COSMIC measurements over the equatorial and low-latitude regions of the nearly Indian continent (~Geog. 5–40°N and 60–100°E) for the complete mission period. The study is further extended for the evaluation of the IRI-2012 model. The main conclusions are summarized as follows:

4.1. NmF2

(a) Stronger EIA in summer and winter during high solar activity and in all years in equinoxes is observed.
(b) A clear solar activity dependence is observed and NmF2 increases with increase in solar activity over both latitudes throughout the day.
(c) Post-sunset (~1800 LT) enhancement is strong over equatorial-low latitude during 2010–2011 period in winter and over equator in equinoxes during all

phases of solar activity respectively whereas a post-midnight enhancement occurs over both regions during high solar activity phases and the strength increases with the increase in solar activity (higher in winter and equinox) respectively.

(d) Day-to-variability (stdev) is lower during nighttime and increases during high solar activity. Both VI and RV is lower during noontime in all seasons over both latitudes whereas is higher during morning hours (equator-low latitude) and nighttime (low-latitude) respectively.

(e) Winter anomaly over equator is absent and weak during low (2006–2009) and high (2010–2013) solar activity period whereas over low-latitude, is stronger in low and moderate phase (2006–2007 and 2010–2011) but absent in minimum and maximum (2008–2009 and 2012–2013) solar activity period respectively. The semi-annual anomaly is present irrespective of solar activity over both regions but stronger for low-latitude respectively.

4.2. hmF2

(a) hmF2 varied from 230 km to 415 km for equator and 220 km to 340 km for low-latitude (noontime: 310 km to 415 km and 235 km to 350 km for equator and low-latitude) respectively is higher over equator throughout the day in general irrespective of season and solar activity. However, the noontime peak is even lower than midnight peak in winter over low-latitude.

(b) The stdev ranged between 15 km and 70 km throughout the period over both latitude and seasons respectively. The VI and RV is higher in morning (30%) for summer and 20% for other times of day for equator whereas is higher (∼30% and 25%) during noontime over low-latitude respectively.

4.3. COSMIC observations and IRI

(a) IRI-2012 modeled values followed well the general trend for seasons using both models for NmF2 and hmF2, however, the quantitative discrepancies exists. The noontime modeled NmF2 is more in agreement by CCIR (discrepancy ∼ 50%) compared to URSI (discrepancy ∼ 90%) for both equatorial-low latitude. But higher discrepancy existed in NmF2 for nighttime and morning for equator whereas is higher throughout the day for low-latitude. The predicted hmF2 exhibited a smaller discrepancy (<20%) throughout the day.

(b) The model is strongly correlated for NmF2 by CCIR ($r^2 \sim 0.93$ and 0.94) and URSI (∼0.90 and 0.93). The model over-/under-estimated over equatorial/low-latitude region in different seasons respectively. The overall correlation for hmF2 using complete data-set is moderate by both models and latitudes (0.56–0.62) with overestimation up to ∼96 km. The correlation for each season is strong/moderate over equatorial/low-latitude respectively. In conclusion, we found CCIR more in agreement to the observed values for the equatorial-low latitude regions.

Some of our reported results using COSMIC observations are in agreement with previous studies using the ground-based ionosondes in the Indian regions. The results presented here give view point for the corrections needed in the model for the equatorial and low-latitude region. The NmF2 and hmF2 in the equatorial and low-latitude ionosphere exhibits considerable day-to-day variability and is still a crucial challenge for the sophisticated models of the upper atmosphere. It should be pointed out that this work of examining the variability of the ionospheric parameters using satellite-based COSMIC measurement is the first time effort to reveal the characteristics of ionospheric behavior for varying solar activities in the Indian sector. Hence more studies using ground based measurements at sites are planned for the near future with the investigation of factors other than the solar activity which may also be responsible for these variabilities.

Acknowledgement

MA is grateful to the Department of Science and Technology (DST)-SERB, India for awarding the Ramanujan Fellowship during the study period. She is also grateful to Prof. D.S. Ramesh, Director of IIG, Mumbai for providing the hosting facilities at the Institute. The OMNI website for geomagnetic and interplanetary data, the CELIAS/SEM experiment on SOHO spacecraft for EUV fluxes and COSMIC data (http://www.cosmic.ucar.edu/) are also highly acknowledged for making the data available online. We acknowledge the IRI team members for regularly updating, maintaining and making online for users. The authors are grateful to the Potential Reviewers for their very careful corrections, comments and suggestions which have helped in improving the manuscript.

References

Abdu, M.A., 2005. Equatorial ionosphere thermosphere system: electrodynamics and irregularities. Adv. Space Res. 35 (5), 771–787.

Aggarwal, M., Joshi, H.P., Iyer, K.N., 2007. Solar activity dependence of electron and ion temperatures using SROSS C2 RPA data and comparison with IRI model. J. Atmos. Sol.-Terres. Phys. 69 (7), 860–874.

Aggarwal, M., Joshi, H.P., Iyer, K., Jivani, M., 2009. Studies of electron and ion temperatures at 500 km altitude during sunrise using Indian SROSS C2 satellite. Adv. Space Res. 43 (2), 273–281.

Aggarwal, M., 2011. TEC variability near northern EIA crest and comparison with IRI model. Adv. Space Res. 48 (7), 1221–1231.

Aggarwal, M., Joshi, H.P., Iyer, K.N., Kwak, Y.-S., Lee, J.J., Chandra, H., Cho, K.S., 2012. Day-to-day variability of equatorial anomaly in

GPS-TEC during low solar activity period. Adv. Space Res. 49, 1709–1720.
Azzarone, A., Bianchi, C., Pezzopane, M., Pietrella, M., Scotto, C., Settimi, A., 2012. IONORT: a Windows software tool to calculate the HF ray tracing in the ionosphere. Comput. Geosci. 42, 57–63.
Batista, I.S., Abdu, M.A., 2004. Ionospheric variability at Brazilian low and equatorial latitudes: comparison between observations and IRI model. Adv. Space Res. 34, 1894–1900.
Bilitza, D., 2001. International reference ionosphere 2000. Radio Sci. 36, 261.
Bilitza, D., Reinisch, B.W., 2008. International Reference Ionosphere 2007: improvements and new parameters. Adv. Space Res. 42 (4), 599–609.
Bilitza, D., Altadill, D., Zhang, Y., Mertens, C., Truhlik, V., Richards, P., McKinnell, L.-A., Reinisch, B., 2014. The International Reference Ionosphere 2012 - a model of international collaboration. J. Space Weather Space Climate 4 (A07), 12.
Bilitza, D., 2014. The International Reference Ionosphere: Rawer's IRI and its status today. Adv. Radio Sci. 12, 231–236.
Bramley, E.N., Margaret, Y., 1968. Winds and electromagnetic drifts in the equatorial F2-region. J. Atmosp. Terres. Phys. 30 (1), 99–111.
Brum, C.G.M., Rodrigues, F.Da.S., Dos, Pedrina T., Matta, A.C., Aponte, N., Gonzalez, S.A., Robles, E., 2011. A modeling study of foF2 and hmF2 parameters measured by the Arecibo incoherent scatter radar and comparison with IRI model predictions for solar cycles 21, 22, and 23. J. Geophys. Res.: Space Phys. 116 (A3), CiteID A03324.
Chauhan, V., Singh, O.P., 2010. A morphological study of GPS-TEC data at Agra and their comparison with the IRI model. Adv. Space Res. 46, 280–290.
Chu, Yen-Hsyang, Su, Chin-Lung, Ko, Hsiao-Tsung, 2010. A global survey of COSMIC ionospheric peak electron density and its height: a comparison with ground-based ionosonde measurements. Adv. Space Res. 46 (4), 431–439.
Chuo, Y.J., Lee, C.C., 2008. Ionospheric variability at Taiwan low latitude station: comparison between observations and IRI-2001 model. Adv. Space Res. 42 (4), 673–681.
Ezquer, R.G., Mosert, M., 2007. Ionospheric variability studies in Argentina. Adv. Space Res. 39 (5), 949–961.
Hajj, George A., Romans, Larry J., 1998. Ionospheric electron density profiles obtained with the Global Positioning System: results from the GPS/MET experiment. Radio Sci. 33 (1), 175–190.
Hanson, W.B., Patterson, T.N.L., 1964. The maintenance of the night-time F-layer. Plan. Space Sci. 12 (10), 979–997.
Huang, Y.N., Cheng, K., Chen, S.W., 1989. On the equatorial anomaly of the ionospheric total electron content near the northern anomaly crest. J. Geophys. Res. 94, 13515–13525.
Judge, D.L., McMullin, D.R., Ogawa, H.S., Hovestadt, D., Klecker, B., Hilchenbach, M., Mobius, E., Canfield, L.R., Vest, R.E., Watts, R., Tarrio, C., Kuehne, M., Wurz, P., 1998. First solar EUV irradiances obtained from SOHO by the CELIAS/SEM. Sol. Phys. 177 (1/2), 161–173.
Kane, R.P., 1992. Solar cycle variation of foF2. J. Atmosp. Terres. Phys. 54 (9), 1201–1205 (ISSN 0021-9169).
Karami, Kh., Ghader, S., Raeen, A., 2011. Comparison of peak characteristics of F2 ionospheric layer over Tehran region at a low solar activity period with IRI-2001 and IRI-2007 models predictions. Adv. Space Res. 48 (6), 1049–1055.
Karia, S.P., Patel, N.C., Pathak, K.N., 2015. Comparison of GPS based TEC measurements with the IRI-2012 model for the period of low to moderate solar activity (2009–2012) at the crest of equatorial anomaly in Indian region. Adv. Space Res. 55, 1965–1975.
Kawamura, S., Balan, N., Otsuka, Y., Fukao, S., 2002. Annual and semiannual variations of the midlatitude ionosphere under low solar activity. J. Geophys. Res. 107, A81166. http://dx.doi.org/10.1029/2001JA000267.
Klobuchar, J., 1986. Design and characteristics of the GPS ionospheric time delay algorithm for single frequency users. In: Proceedings of PLANS'86 – Position Location and Navigation Symposium, Las Vegas, Nevada, 4–7 November, pp. 280–286.
Kohl, H., King, J.W., 1967. Atmospheric winds between 100 and 700 km and their effects on the ionosphere. J. Atmos. Terres. Phys. 29 (9), 1045–1062.
Liu, L., Wan, W., Ning, B., Pirog, O.M., Kurkin, V.I., 2006. Solar activity variations of the ionospheric peak electron density. J. Geophys. Res. 111, A08304. http://dx.doi.org/10.1029/2006JA011598.
Maltseva, O.A., Mozhaeva, N.S., Poltavsky, O.S., Zhbankov, G.A., 2012. Use of TEC global maps and the IRI model to study ionospheric response to geomagnetic disturbances. Adv. Space Res. 49, 1076–1087.
Miller, K.L., Torr, D.G., Richards, P.G., 1986. Meridional winds in the thermosphere derived from measurement of F2 layer height. J. Geophys. Res. 91, 4531–4535.
Miller, K.L., Lemon, M., Richards, P.G., 1997. A meridional wind climatology from a fast model for the derivation of meridional winds from the height of the ionospheric F2-region. J. Atmos. Sol. Terr. Phys. 59, 1805–1822.
Mukherjee, S., Sarkar, S., Purohit, P.K., Gwal, A.K., 2010. Seasonal variation of total electron content at crest of equatorial anomaly station during low solar activity conditions. Adv. Space Res. 46 (3), 291–295.
Pavlov, A.V., Pavlova, N.M., 2005. Causes of the mid-latitude NmF2 winter anomaly at solar maximum. J. Atmosp. Sol.-Terres. Phys. 67 (10), 862–877.
Rama Rao, P.V.S., Niranjan, K., Prasad, D.S.V.V.D., Gopi Krishna, S., Uma, G., 2006. On the validity of the ionospheric pierce point (IPP) altitude of 350km in the Indian equatorial and low-latitude sector. Ann. Geophys. 24, 2159–2168.
Rastogi, R.G., Klobuchar, J.A., 1990. Ionospheric electron content within the equatorial F2 layer anomaly belts. J. Geophys. Res. 95, 19045–19052.
Rathore, V.S., Kumar, Singh, Singh, A.K., 2015. A statistical comparison of IRI TEC prediction with GPS TEC measurement over Varanasi, India. J. Atmos. Sol.-Terres. Phys. 124, 1–9.
Rawer, K., Bilitza, D., Ramakrishnan, S., 1978. Goals and status of international reference ionosphere. Rev. Geophys. 16, 177–181.
Richards, P.C., Fennelly, J.A., Torr, D.G., 1994a. EUVAC: a solar EUV flux model for aeronomic calculations. J. Geophys. Res. 99 (A5), 8981–8992.
Richards, P.G., Torr, D.G., Buonsanto, M.J., Sipler, D.P., 1994b. Ionoshperic effects of the March 1990 magnetic storm: comparison of theory and measurement. J. Geophys. Res. 99 (A12), 23359–23365 (ISSN 0148-0227).
Richards, P.G., 2001. Seasonal and solar cycle variations of the ionospheric peak electron density: comparison of measurement and models. J. Geophys. Res. 106 (A7), 12803–12820.
Rishbeth, H., Garriot, O.K., 1969. Introduction to Ionospheric Physics. Academic Press, New York..
Rishbeth, H., Müller-Wodarg, I.C.F., Zou, L., Fuller-Rowell, T.J., Millward, G.H., Moffett, R.J., Idenden, D.W., Aylward, A.D., 2000. Annual and semiannual variations in the ionospheric F2-layer: II. Physical discussion. Ann. Geophys. 18 (8), 945–956.
Rush, C., Fox, M., Bilitza, D., Davies, K., Mcnamara, L., Stewart, F., Pokempner, M., 1989. Ionospheric mapping – an update of foF2 coefficients. Telecomm. J. 56, 179–182.
Scherliess, L., Fejer, B.G., 1999. Radar and satellite global equatorial F region vertical drift model. J. Geophys. Res. 104 (A4), 6829–6842.
Schreiner, W.S., Sokolovskiy, S.V., Rocken, C., Hunt, D.C., 1999. Analysis and validation of GPS/MET radio occultation data in the ionosphere. Radio Sci. 34 (4), 949–966.
Schreiner, W., Rocken, C., Sokolovskiy, S., Syndergaard, S., Hunt, D., 2007. Estimates of the precision of GPS radio occultations from the COSMIC/FORMOSAT-3 mission. Geophys. Res. Lett. 34 (4), CiteID L04808.
Sethi, N.K., Mahajan, K.K., 2002. The bottomside parameters B0, B1 obtained from incoherent scatter measurements during a solar

maximum and their comparisons with the IRI-2001 model. Ann. Geophys. 20 (10), 1677–1685.

Sethi, N.K., Dabas, R.S., Vohra, V.K., 2004. Diurnal and seasonal variations of hmF2 deduced from digital ionosonde over New Delhi and its comparison with IRI 2001. Ann. Geophys. 22, 453–458.

Sethi, N.K., Dabas, R.S., 2006. Diurnal and seasonal variations of bottomside profile parameters B0, B1 during high solar activity at New Delhi and their comparisons with IRI-2001 model. In: 36th COSPAR Scientific Assembly. Held 16–23 July 2006, in Beijing, China. Meeting abstract from the CDROM, #2294.

Sethi, N.K., Dabas, R.S., Ninawe, Y., 2007. FoF2 variability over New Delhi during different solar cycle conditions and comparison with IRI-2001 model. Adv. Space Res. 40 (6), 855–860.

Sharma, Som, Chandra, H., Vyas, G.D., 1999. Long term ionospheric trends over Ahmadabad. Geophys. Res. Lett. 26 (3), 433–436.

Sharma, D.K., Rai, J., Israil, M., Subrahmanyam, P., 2005. Diurnal, seasonal and latitudinal variations of ionospheric temperatures of the topside F region over the Indian region during solar minimum (1995–1996). J. Atmosp. Sol.-Terres. Phys. 67 (3), 269–274.

Sharma, P.K., Pathak, P.P., Sharma, D.K., Rai, J., 2010. Variation of ionospheric electron and ion temperatures during periods of minimum to maximum solar activity by the SROSS-C2 satellite over Indian low and equatorial latitudes. Adv. Space Res. 45 (2), 294–302.

Sharma, D.K., Aggarwal, M., Bardhan, A., 2016. Variability of ionospheric parameters during solar minimum and maximum activity and assessment of IRI model. Adv. Space Res. http://dx.doi.org/10.1016/j.asr.2016.11.0 (in press).

Sobral, J.H.A., Abdu, M.A., Muralikrishna, P., Labelle, J., Castilho, Vivian M., Zamlutti, C.J., 2003. Rocket and ground-based electron density soundings versus IRI representation. Adv. Space Res. 31 (3), 569–575.

Sripathi, S., 2012. COSMIC observations of ionspheric density profiles over Indian region: ionospheric conditions during extremely low solar activity period. Indian J. Radio Space Phys. 41, 98–109.

Syndergaard, S., Schreiner, W.S., Rocken, C., Hunt, D.C., Dymond, K. F., 2006. Preparing for COSMIC: inversion and analysis of ionospheric data products. In: Foelsche, U., Kirchengast, G., Steiner, A.K. (Eds.), Atmosphere and Climate: Studies by Occultation Methods. Springer, New York, pp. 137–146.

Walker, G.O., 1971. Electron content and topside plasma temperature studies at low latitudes during a period from sunspot minimum to sunspot maximum. J. Atmosp. Terres. Phys. 33, 1041–1053.

Wang, X., Shi, J.K., Wang, G.J., Gong, Y., 2009. Comparison of ionospheric F2 peak parameters foF2 and hmF2 with IRI2001 at Hainan. Adv. Space Res. 43, 1812–1820.

Wichaipanich, N., Supnithi, P., Ishii, M., Maruyama, T., 2010. Ionospheric variation at Thailand equatorial latitude station: comparison between observations and IRI-2001 model predictions. Adv. Space Res. 45 (2), 284–293.

Wu, C.C., Fryb, C.D., Liu, J.-Y., Lioud, K., Tsenge, C.-L., 2004. Annual TEC variation in the equatorial anomaly region during the solar minimum: September 1996–August 1997. J. Atmosp. Sol.-Terres. Phys. 66, 199–207.

Yadav, S., Dabas, R.S., Das, Rupesh M., Upadhayaya, A.K., Sharma, K., Gwal, A.K., 2010. Diurnal and seasonal variation of F2-layer ionospheric parameters at equatorial ionization anomaly crest region and their comparison with IRI-2001. Adv. Space Res. 45 (3), 361–367.

Yue, X., Schreiner, W.S., Lei, J., Sokolovskiy, S.V., Rocken, C., Hunt, D. C., Kuo, Y.-H., 2010. Error analysis of Abel retrieved electron density profiles from radio occultation measurements. Ann. Geophys. 28, 217–222.

Zeng, Z., Burns, A., Wang, W., Lei, J., Solomon, S., Syndergaard, S., Qian, L., Kuo, Y.H., 2008. Ionospheric annual asymmetry observed by the COSMIC radio occulation measurements and simulated by the TIEGCM. J. Gophys. Res. 113, A07305. http://dx.doi.org/10.1029/2007JA012897.

Zhang, M.-L., Shi, J.-K., Wang, X., Shang, S.-P., Wu, S.-Z., 2007. Ionospheric behavior of the F2 peak parameters foF2 and hmF2 at Hainan and comparisons with IRI model predictions. Adv. Space Res. (5), 661–667